applied sciences

MDPI

Article

M13 Phages Uptake of Gold Nanoparticles for Radio- and Thermal-Therapy and Contrast Imaging Improvement

Lorenzo Torrisi [1,*], Letteria Silipigni [1], Lubomir Kovacik [2], Vasily Lavrentiev [3], Mariapompea Cutroneo [3], Alfio Torrisi [4,*], Laura Maria De Plano [5], Domenico Franco [5] and Salvatore Guglielmino [5]

1 Department of Mathematical and Computer Sciences, Physical Sciences and Earth Sciences, MIFT, University of Messina, V.le F.S. d'Alcontres 31, S. Agata, 98158 Messina, Italy; letteria.silipigni@unime.it
2 Center for Cellular Imaging and NanoAnalytics (C-CINA) Biozentrum, University of Basel, CH-4058 Basel, Switzerland; lubomir.kovacik@unibas.ch
3 Nuclear Physics Institute, Czech Academy of Sciences, 25068 Řež, Czech Republic; lavrentiev@ujf.cas.cz (V.L.); cutroneo@ujf.cas.cz (M.C.)
4 Department of Mathematics and Physics "E. De Giorgi"-CEDAD (CEnter of Applied Physics, DAting and Diagnostics), University of Salento, 73100 Lecce, Italy
5 Department of Biological and Environmental Sciences, University of Messina, V.le F.S. d'Alcontres 31, 98158 Messina, Italy; lauramaria.deplano@unime.it (L.M.D.P.); domenico.franco@unime.it (D.F.); salvatore.guglielmino@unime.it (S.G.)
* Correspondence: ltorrisi@unime.it (L.T.); alfio.torrisi@unisalento.it (A.T.)

Abstract: The presented work deals with the uptake of gold nanoparticles (Au NPs) by M13 phages in solutions. In particular, the Au NPs uptake modalities and their localization in the filamentous phages are evaluated and measured. Gold spherical nanoparticles (with an average diameter of the order of 10 nm) are obtained by laser ablation in water with a sodium citrated surfactant. The interest of such application comes from the possibility to employ living biological structures to transport heavy metallic nanoparticles inside cells of tumoral tissues. Indeed, phages have the capability to introduce Au NPs in the proximity to the cell nucleus, increasing the efficiency of DNA destruction in the tumoral cells by employing low doses of ionizing radiation during radiotherapy and hyperthermia treatments. Several analyses and microscopy characterizations of the prepared phages samples embedding gold nanoparticles are presented, demonstrating that the presence of Au NPs increases the phages imaging contrast.

Keywords: gold nanoparticles; hyperthermia; M13 phages; radiotherapy

Citation: Torrisi, L.; Silipigni, L.; Kovacik, L.; Lavrentiev, V.; Cutroneo, M.; Torrisi, A.; De Plano, L.M.; Franco, D.; Guglielmino, S. M13 Phages Uptake of Gold Nanoparticles for Radio- and Thermal-Therapy and Contrast Imaging Improvement. *Appl. Sci.* **2021**, *11*, 11391. https://doi.org/10.3390/app112311391

Academic Editor: Fabrice Goubard

Received: 25 October 2021
Accepted: 29 November 2021
Published: 1 December 2021

1. Introduction

M13 phage, 880 nm long and 6.6 nm wide, is a virus consisting of ~2700 copies of the major coat protein (pVIII), surrounding a single-stranded DNA [1,2]. Its properties, such as high sensitivity to ultrasonication and stability under different conditions, such as organic solvents [1], allow it to be employed for different applications in virotronics, as well as in electronics [3], for the development of optical biosensors [4,5] and for medical devices [6]. Specifically, the use of phages in human applications have increased researchers' interest due to their absence of tropism for mammalian cells and innate ability to cross biological membranes, such as vascular endothelium and other mammalian cell barriers [7,8]. It has been demonstrated that phages rapidly translocate throughout the body upon administration, with a distribution that depends on the route of administration and initial phage titer [7,8]. The distribution in a specific tissue can be increased by the phage display technology that allows to display peptide able to specifically bind eukaryotic cells [9,10]. Moreover, phages can be easily internalized by receptor-mediated endocytosis if they display an internalizing peptide [7].

M13 phages can be used to promote the nucleation of specific inorganic materials with a high level of selectivity and control [11] or for templating inorganic nanoparticles. Based

on the covalent chemical bonds, following a self-assembly approach, gold nanoparticles (Au NPs) prepared by laser ablation, following the so-called top-down method, can be embedded into M13 phages [12]. The literature reports that the surface-enhanced Raman scattering (SERS) nanoprobe based on the M13 phages exhibits bactericidal capabilities and can be employed for the selective detection and inactivation of *Staphylococcus aureus* [13]. Moreover, M13 phages fitted together with metallic nanoparticles of Ag or Au, can be employed to modify the cytotoxicity in healthy and tumor cells generating conditions for cell apoptosis [12,14]. Such studies highlight how the use of M13 phages with heavy metallic nanoparticles can open new and interesting avenues in tumor targeting for its treatment.

In this work, it is investigated the affinity of M13 phages to Au NPs by means of different microscopy techniques, such as SEM (scanning electron microscopy), AFM (atomic force microscopy) and TEM (transmission electron microscopy) and by complementary analyses, such as EDX (energy dispersive X-ray spectroscopy), UV–VIS absorption and Raman spectroscopies. The goal of the study consists of the preparation of phage cultures to transport metallic nanoparticles toward specific tumoral tissues and to use them as a contrast medium, increasing the imaging contrast for the radiotherapy diagnostic and biological studies.

Gold is a biologically compatible element because it is an inert noble metal and is thermally and chemically stable [15]. Due to the increasing of the effective atomic number of the organs and tissues in which the Au NPs will be located, a significant increment of the radiotherapy efficiency and of hyperthermia and imaging improvement are expected [16]. Nano-and microstructures bonded to Au NPs can be better highlighted, thanks to the fluorescence emission and optical spectroscopy of heavy nanoparticles [17]. Moreover, the rising of light absorption at specific wavelengths due to the presence of Au NPs, known as surface plasmon resonance (SPR) [18], represents an important effect in hyperthermia, destroying the cancer cells inducing controllable heating.

2. Materials and Methods

2.1. Au NPs Preparation

A Nd:YAG laser (1064 nm wavelength, 3 ns pulse width, 50 mJ pulse energy, 10 Hz repetition rate), was focused on a pure gold target (99.99%), placed into a glass tube filled with distilled water. The focused laser spot on the target was equal to 1 mm^2, irradiating with a fluence of 5 J/cm^2 and an intensity of about 3×10^9 W/cm^2. The target surface was placed at 4 mm depth in the water and the volume of the liquid ranged between 1 cm^3 and 2 cm^3. The target moves during the laser irradiation due to the shock waves induced by the laser pulses; this changes the position of the laser ablation surface, producing a uniform erosion of the target surface in order to obtain a uniform production of the Au NPs in the liquid, as described in more detail in previous papers [19].

The pulse laser generated plasma, not being able to expand due to the over imposed liquid, is produced at the solid–liquid interface and gives rise to gas bubbles, which expand in the liquid up to their implosion with the release of nanoparticles.

Inside the bubble, before its implosion, high interaction between the energetic ions and the neutral species occurs with clusters and nanoparticles nucleation. The nanoparticles are released in the liquid having a volume delimited by the glass tube section (3.14 cm^2) and by the water level in the glass of about 1.6 cm. Thus, the nanometric gold particles are dispersed in a liquid volume of about 5 cm^3. The difference in weight of the small Au target before and after the total laser irradiation allows to evaluate the ablation yield, which is generally of the order of 50 ng/pulse. With an irradiation of 33 min, a total ablation mass of 1 mg is produced, and the concentration of the Au NPs solution in water is of about 1 mg/cm^3. Thus, fixing the laser parameters, the solution concentration depends on the irradiation time, which generally ranges between 15 min and 45 min.

Figure 1 shows the pulsed laser during the Au NPs production in water (a), the scheme of the experimental set-up (b), the absorbance measurements of the prepared solution of Au NPs with an average size of 20 nm in water (c), and the generated nanoparticles diameter

distribution evaluated by using TEM microscopy (d). The absorbance peak reported in Figure 1c, centered at ~520 nm wavelength, is due to the surface plasmon resonance (SPR) induced by the incident light on the metallic nanoparticles, which increases the light absorbance proportionally to the size of the conductive spherical nanoparticle [20].

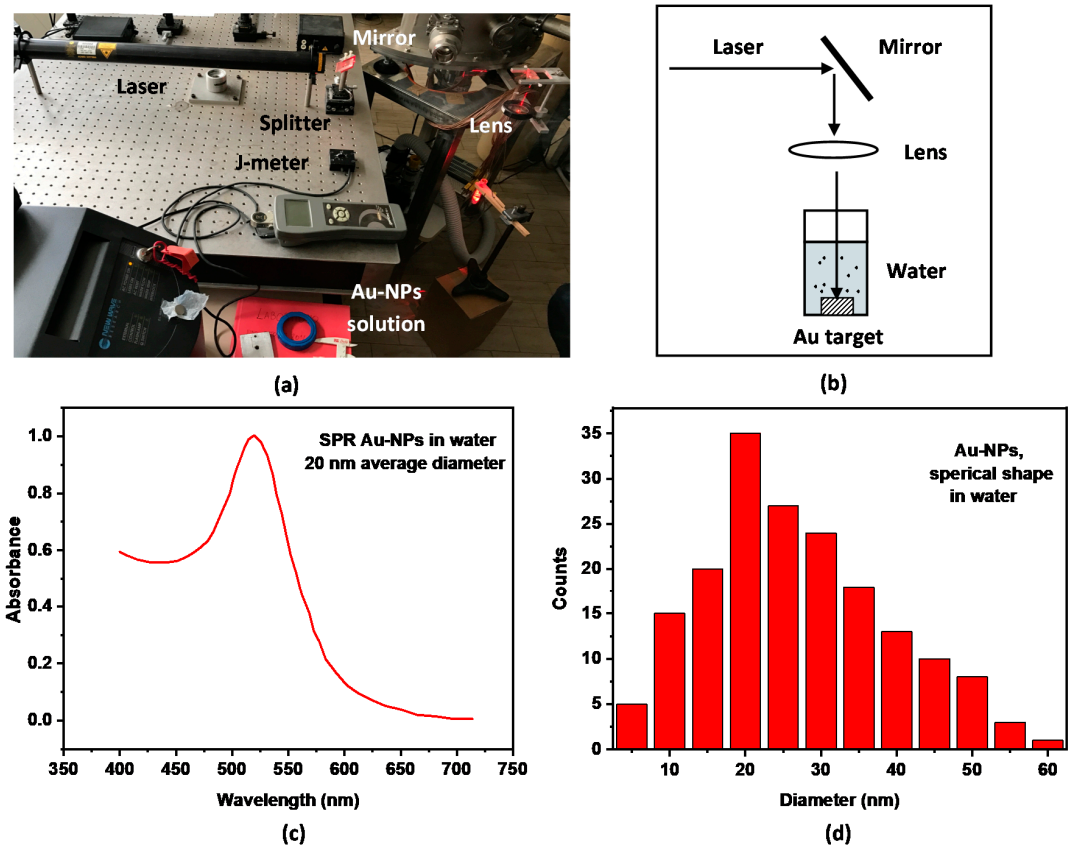

Figure 1. Experimental set-up photo (**a**), scheme of the Au NPs production by laser (**b**), measurement of absorbance vs. wavelength (**c**) and produced Au NPs diameter distribution (**d**).

2.2. M13 Phages Production

The M13 phages (helper phage M13K07, Kan+) were propagated in the bacterial host Escherichia coli strain TG1 (Kan-, Amp-, lacZ-), grown in modified Luria–Bertani broth (LB) medium (10 g/L tryptone, 5 g/L yeast extract, 5 g/L NaCl) added with kanamycin (10 mg/L). The culture was incubated overnight at 250 rpm in an orbital shaker (ARGO lab SKO-DXL) at 37 °C. After the incubation, the phage particles were recovered from the bacterial host culture by means of several centrifugation steps in PEG/NaCl solution, containing 200 g PEG-8000 (polyethylene glycol; Sigma-Aldrich, Milan, Italy) and 150 g NaCl (Sigma-Aldrich, Milan, Italy) per liter. Specifically, the culture was centrifuged at 8000× *g* for 20 min at 25 °C; the supernatant was recovered and mixed with 25% (*v*/*v*) of PEG/NaCl solution. The mixture was cooled in ice for 4 h and precipitated by centrifugation at 15,000× *g* for 45 min at 4 °C. The pellet was recovered, resuspended in 10% (*v*/*v*) of TRIS buffered saline (TBS, 7.88 g/L of Tris hydrochloride and 8.77 g/L of NaCl in deionized water), mixed again with 25% (*v*/*v*) of PEG/NaCl, cooled in ice for 4 h, and the solution was centrifuged as above. The pellet, containing phage particles, was suspended in 10% (*v*/*v*) of TBS, filtered through 0.22 µm pore size membrane (Millipore), and stored at 4 °C. The M13 phage concentration was deduced by tenfold serial dilutions. Specifically, 10 µL from each dilution sample was dispensed into sterile micro-centrifuge tubes containing 90 µL of *E. coli* TG1 culture at OD600 equal to 0.7. Tubes were incubated at 37 °C in a static condition for 15 min and at 250 rpm on a rotary shaker for 20 min.

After the incubation, 100 µL of each phage/E. coli TG1 suspension was dispensed into LA plates containing kanamycin (10 µg/mL) and incubated at 37 °C overnight. Plates, containing between 30 and 300 colonies, were counted to derive the number of active viral particles able to infect the host cell and express the transgene. Thus, the active particles were determined by transducing units per milliliter (TU/mL), according to the following Equation (1):

$$\frac{\text{TU}}{mL} = \frac{(\text{number of colonies})}{\text{volume } (0.1 \text{ m}L) \times \text{ dilution factor}} \quad (1)$$

2.3. Preparation of Au NPs@TA Nanoparticles

In order to allow binding with phages, the Au NPs were modified by thioctic acid (TA), according to Volkert with some modifications [21]. The Au NPs solution, filtered by a 0.45 µm filter to remove any aggregate, was adjusted at pH = 11 with 1 M NaOH. Then, 1 mL of the 10 nM Au NPs solution was added with 0.1 mL of 10 mM TA ethanolic solution (*v/v* ratio of 1 to 10). The mixture solution was stirred at 20 °C in the dark for at least 16 h. After this period, the TA excess was removed by 11,500× g for 20 min, and Au NPs@TA was resuspended in distilled water and kept at 4 °C.

2.4. Preparation of Au NPs@TA@phages

The M13 phages embedding was mediated by TA covering Au NPs. In fact, Au NPs@TA, prepared as above, exposes free carboxylic acid groups able to covalently bind the M13 phages amine groups by the carbodiimide linkage. For this purpose, the 10 nM Au NPs@TA was washed twice with 1 mL of 2-(N-morpholino) ethanesulfonic acid (MES) buffer (pH 6.0) by alternating steps of stirring and centrifugation at 11,500× g for 20 min and resuspended in the 0.25 mL MES buffer containing 10 mg 1-ethyl-3 [3-dimethylaminopropyl] carbodiimide (EDC). Then, the activated Au NPs@TA was added to 100 µL of the M13 phage (10^{12} TU/mL) and incubated in a rotator shaker for 2 h at rt. After the incubation, the supernatants were discarded and Au NPs@TA@phage was washed thrice with phosphate buffer saline (PBS) (pH 7.1) and kept at 4 °C.

2.5. Microscopy Analyses of M13-Phages

TEM images of the prepared samples were acquired by a FEI Talos TEM with a FEG gun operating at 200 kV and a FEI Ceta CMOS camera with an exposure of 1 s.

SEM images were acquired using a field emission scanning electron microscope FE-SEM ZEISS Merlin with Gemini II® column, at an acceleration voltage of 10 kV. Before the analysis, the samples were deposited (as drops) on a clean mirror aluminum substrate, dried in air at 30 °C for 1 h, and successively put in vacuum at a pressure of 1 mbar for 24 h, without any metallization.

EDX spectroscopy (energy dispersive X-ray spectroscopy) coupled to the SEM microscope operating with a 5 keV electron beam allowed to obtain information about the Kα lines of B, C, N, and O, as well as about the Au NPs characteristic M-lines in a range of energy from 183 eV to 5 keV. Sweeping the electron gun, it was possible to record the distribution spectra of the characteristic X-rays of Au and of other elements present in the sample surface.

AFM topography measurements were carried out in the non-contact mode, at room temperature and ambient pressure, with a Nanosurf microscope (AG, Liestal, Switzerland) having a 3 × 3 μm^2 scanning area and relative zooms. Measurements were accomplished with Si cantilever tips (Nanoworld AG, Liestal, Switzerland) at a constant force of 48 N/m and with a resonance frequency of 190 kHz.

The optical absorption response of the Au NPs in the solution was performed, employing a PerkinElmer LAMBDA 25 UV–VIS double-beam spectrometer, operating in the 210–800 nm wavelength range. The employed radiation source consists of a tungsten, halogen and deuterium lamps combination with an automatic light source change at about 326 nm wavelength. Furthermore, few solution drops, containing the prepared phages

with Au NPs, were deposited on silicon substrates, and once dried, were analyzed by a Horiba-Jobin Yvon Raman system (model HR800) equipped with a confocal microscope, using the 633 nm emission from a helium–neon laser.

3. Results

Samples with a high phage concentration (10^{12} TU/100 µL) were prepared for the SEM analysis, depositing microdrops on a thin Cr metallization film to avoid charge accumulation during the microscope observation. It was possible to observe the assembled M13 phages with Au NPs, deposited on polished silicon substrates, at different magnifications. In the acquired images, it is possible to see, mainly, the solution salts and micrometric agglomerations with no perception of the phage filamentation. Au NPs are observed at the highest magnification of 70,000×. The image quality was improved, employing an aluminum polished substrate. Additionally, in this case, it was not possible to observe the single nanoparticles (of the order of 10 nm) but only near-spherical aggregated particles (of the order of 200 nm or larger), as shown in Figure 2a, and the global characteristic spectrum of the elements present in the observed zone (Figure 2b). The EDX analysis performed on the area confirms the presence of Au NPs by the gold X-ray characteristic M lines, as it is possible to observe from the shown spectrum. It is even possible to observe the characteristic peaks of C, O, Na, and Si, typical elements of both the phage solution and the used substrate. These nanoparticle aggregations may be originated by their addition to the chemical biological molecular environment in the M13 solution or by the sample preparation technique adopted for the sample observation at the electron microscope. The SEM preparation, in fact, needs a thin metallic cover film to make the samples conductive, while, instead, for the TEM observation, it is needed to drip the solution onto a transparent thin polymer film covering a thin metallic grid.

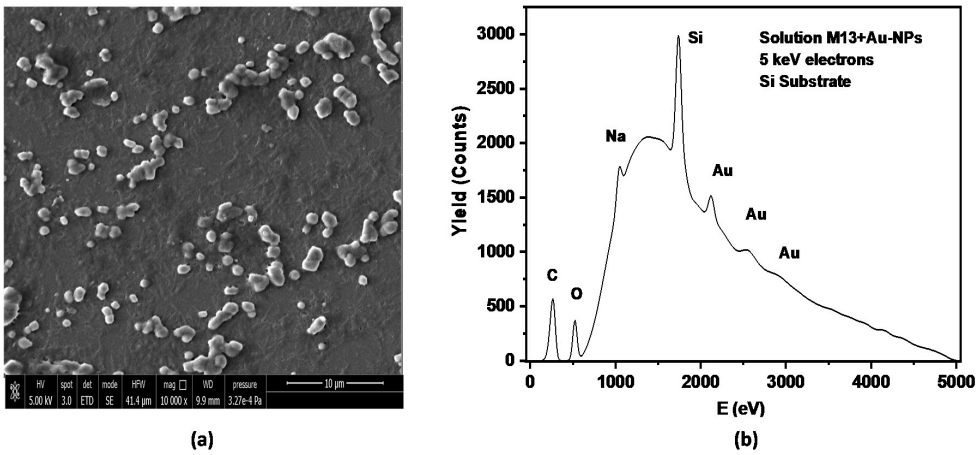

Figure 2. SEM images of the M13 phages with Au NPs compounds (**a**) and relative EDX spectrum of the drops deposited on silicon substrate (**b**).

AFM topographic images allowed to observe the filamentous phage structures. In particular, it was possible observe the Au nanoparticles as white spots, and the phages as whitish traces. In the acquired images, the M13 phages are detected as small peaks (X–ray profile), while the Au NPs are larger and intense peaks in the orthogonal Z dimension. The phages usually include several small nanoparticles along their length. The nanoparticles have a distribution ranging mainly between 10 nm and 100 nm, and the M13 filamentous phages, a length ranging mainly between 0.5 microns and 2 microns and a thickness lower than 10 nm. As it is possible to observe, generally, in each termination of a single phage, 2–8 Au NPs are attached, on average. The Au NPs adhesion to the phages occurs through the protein external layers. Studies of the adhesion of Au NPs with proteins are reported in the literature [22]. In facts, their exposition to biological fluids induces proteins and other biomolecules adsorption onto the surface to form a protein coating sphere around the Au

NPs [23]. The literature reports about the protein interaction with the Au NPs, proposing different biological effects. For example, the protein may be altered by this adhesion to the Au NP and its physiological functions can be modified [24,25].

A series of M13 phages with Au NPs observed by AFM is shown in Figure 3. The first figure (Figure 3a) shows the Au NPs as brilliant nanospheres distributed on an aluminum surface. The average size of the Au NPs is about 10–20 nm ranging between 2 nm and 50 nm. Sometimes the nanoparticles appear joined to each other, especially near the phages, whose proteins may induce nanoparticle coalescence. Far from the phages, the average distance between the nanoparticles is of about 500 nm but near the phages, the average distance decreases and some nanoparticles are in contact. Observing many TEM images, the nanoparticles show thickening when very near the phages. It seems that phages act as attractors of the gold nanoparticles. From two to eight nanoparticles are bonded together with the phage, as it is observable in the detailed contrasted image of Figure 3b (corresponding to the image of phase contrast generally used to highlight the different nature of the materials, thus putting in evidence the metallic nanoparticles with respect to the biological structures) relative to the morphology observation of Figure 3a, which enhances the Au NPs image reducing the contrast of the light elements present in the biological structures. In the background, it is barely possible to observe the phage filamentation, not well resolved and focused, showing a significant density of NPs attached to phages. In this figure, it is possible to observe a phage with about 8 Au NPs (bottom), a second phage with about 10 Au NPs or more (top) and a third phage, to the far left, with more than 5 Au NPs. Some nanoparticles appear larger due to the accumulation of nanoparticles. Generally, the spherical Au NPs are aligned along the phage filamentation, and they are always present in the head and tail of the phage. The AFM images show that the phage filamentation has a length of about 1 micron and a thickness less than 10 nm.

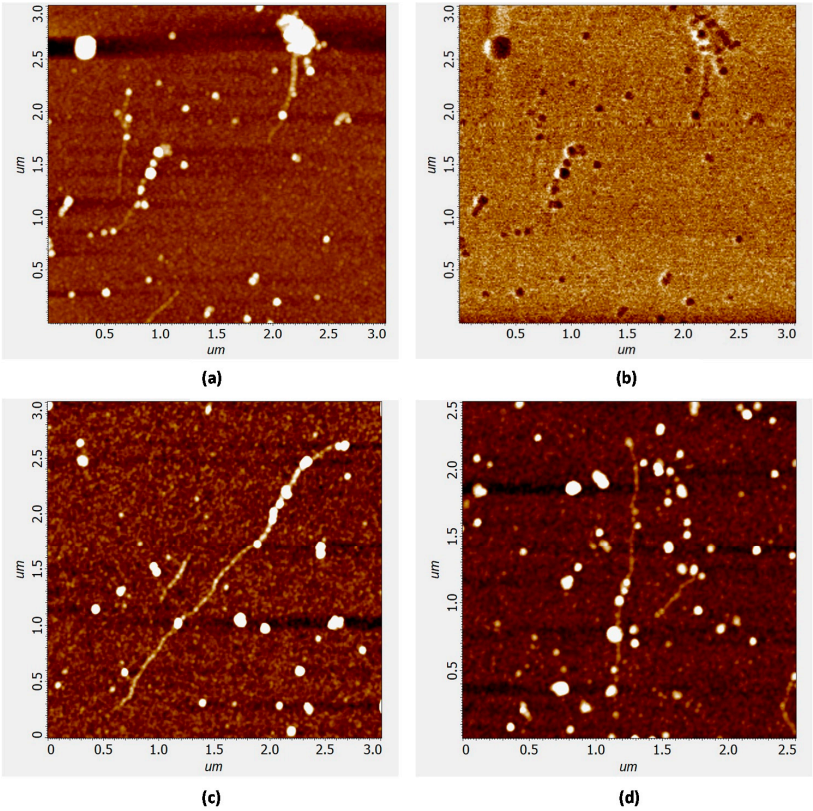

Figure 3. AFM image of Au NPs distribution with respect to phage filamentations (**a**), same image in phase contrast to enhance the Au NPs (**b**), and of single phages showing high number of nanoparticles adherent to them (**c**,**d**).

Figure 3c shows a detailed image of a phage, where the Au NPs near the head are about 20–30 nm distant from one another. The tail contains also small Au NPs but, being out of focus, it is not well resolved. In this case, the phage length is about 2 μm, and 12 nanoparticles are adherent to the phage with a linear density of 12 Au NPs/1 μm. Figure 3d shows another detailed phage of the solution distributed on the Al substrate. It is about 2 m in length and contains Au NPs from 5 nm up to 50 nm in diameter. The nanoparticle linear density on the phage observed in this case is 18 NPs/2 μm.

TEM imaging has allowed to obtain detailed information about the size of Au NPs and M13 phages. It is possible the identification of two main sizes of Au NPs, with dimensions of 10 nm and 50 nm. Moreover, it is observed that, generally, the NPs are attached at the two extremities of the phages, in clusters ranging from 1 to 3 nanoparticles of 10–20 nm each. TEM indicates that the average size of the nanoparticle is equal to 20 nm, while the average phages filamentation length is 1 micron. TEM images are well defined and contrasted by the presence of the heavy metal nanoparticles bonded to the phages surface.

Figure 4 shows four TEM images of single phages and their bonded nanoparticles. The marker length is 10^2 nm. Figure 4a shows a phage with one single Au NP centered with respect to the filamentation and a couple of Au NPs, one bonded to the phage and the other bonded to the first nanoparticle. The phage length and thickness are about 500 nm and 10 nm, respectively, while the Au NP diameter is about 40 nm. The NPs are bonded almost in the center of the filamentation. Figure 4b shows a phage with a NP bonded to the tail and another bonded near the head. In the phage head position is bonded a very little nanoparticle with a dimension comparable with the phage thickness of 10 nm. The small Au NP is less brilliant than the other, due to its lower size. Figure 4c shows a phage at which a single Au-NP with a diameter of about 40 nm is bonded. In turn, this nanoparticle is linked to others, forming a row of more than 4 nanoparticles. Figure 4d shows a phage with a length of about 1 micron at which one nanoparticle is bonding to the head. Observing the filamentation seems that very little NPs, lower than 10 nm, evaluated at about 2 nm, are centered with the filamentation and arranged in alignment with it and equally spaced. A big nanoparticle of about 40 nm is not bonded to the phage, but it may be that the preparation of the sample took place before such adherence occurred.

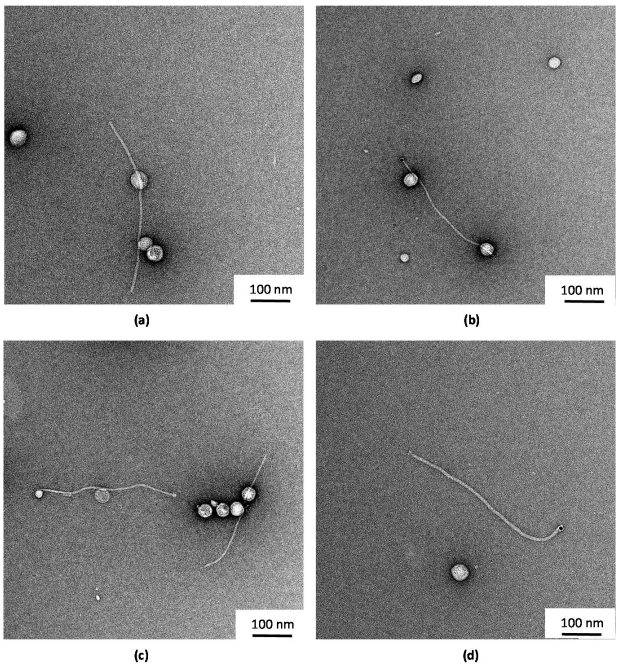

Figure 4. TEM images of single phages with bonded Au NPs in numbers of 2–3 in the centrum (**a**), of 2–3 in the head and tail (**b**), with 4 or more aggregated nanoparticles (**c**) and with low number of NPs of different size in micrometric phage filamentation (**d**).

4. Discussion

Assuming the average phage length of 1 micron and 10 nm thickness, its volume is about 78 $\times$ 10^{-6} μm^3 and, being that its density is about 1 g/cm^3, its weight is about 7.8 $\times$ 10^{-17} g = 0.078 fg. Assuming that, on average, the Au NPs adherent to the phages have a diameter of 40 nm, the volume of the single NP is 3.35 $\times$ 10^4 nm^3 and, being that the Au density is 19.3 g/cm^3, its mass is about 6.37 $\times$ 10^{-16} g= 0.64 fg, i.e., about a factor ten higher than that of the single phage. Because about 4 Au NPs generally are adherent to a single phage, it means that the phages mobility is strongly influenced by the Au NPs that anchor them in the biological substrate and burden the viruses in their diffusion within a biological solution.

At the same time, the Au NPs are aggregated by the phages, reduce their mobility in the solution and can be anchored by the phage filamentation. These aspects find important applications in the field of radiotherapy, hyperthermia and imaging contrast. The high atomic number Z of Au, of 79, is about 5 times higher than that of oxygen and carbon, the main components of biological structures. This higher atomic number determines a high photoelectric cross section μ_{ph} when struck by ionizing radiations since it depends on the following relationship:

$$\sigma_{ph} \propto \frac{Z^4}{h\nu^3} \tag{2}$$

where $h\nu$ is the photon energy. Consequently, the mass absorption coefficient μ_{ph} of the medium can be significantly enhanced by the presence of the heavy Au NPs because

$$\mu_{ph} = \sigma_{ph}\frac{\rho}{A}\,N_A \propto \left(\frac{Z}{h\nu}\right)^3 \tag{3}$$

where ρ is the medium density, A the atomic number, and N_A the Avogadro number.

Thus, the ionization processes employing Au NPs can be enhanced by a factor of up to 600 times higher than for the carbon and oxygen biological elements. The use of Au NPs, also at concentrations lower than 1% in atomic composition, may increase the absorbance of photons inducing the photoelectric effect mainly in the energy range of about 5–500 keV. The Au NPs embedded in different materials, such as in biological fluids, cells and tissues, permit to absorb high photon energy and to modify the properties of the irradiated medium also at relatively low absorbed doses.

Radiotherapy, both using classical X-rays and electron beams and innovative proton and carbon ion beams, represents one important case which reaches the goal to destroy the tumoral cells employing Au NPs transported inside the cells by phages and by diffusive processes. The internalized nanoparticles near the cell nucleus under ionizing irradiation produce high electron emission damaging the DNA of the cell, destroying the cell at absorbed doses lower than the case without Au NPs [26].

To use Au NPs bonded to phages and anchored inside the cell is also advantageous for hyperthermia treatments because the heavy conductive Au element permits to enhance the conduction of heat through the biological fluids. The rate of heat transfer dQ/dt through a material is proportional to the negative gradient in the temperature dT/dx and to the area A through which the heat flows, according to the following heat transport equation:

$$\frac{dQ}{dt} = -kA\frac{dT}{dx} \tag{4}$$

where k is the thermal conductivity of the medium. Thus, although at a low concentration, the insertion of Au NPs having a k conductivity of about a factor 500 times higher than that of water produces a higher heat transfer to the tissues and cells, permitting to damage the tumoral cells containing Au-NPs during hyperthermia cycles for temperatures of about 38–40 °C maintained for times of the order of one hour [27].

Finally, Au NPs can be useful for the image identification of M13 phages and of other biological nanostructures because the heavy element permits to be easily identified by

different fluorescence characteristic lines, which can be detected by high energy resolution detectors. Thus, near nano structures, such as the phages, or macroscopic structures, such as the organs of animals, can be detected thanks to the fluorescence response of Au nanoparticles, for example detecting the L and M characteristic lines of X-ray maps and to the SPR absorption bands in the visible region of optical absorbance spectra [28,29].

Further information about the M13 phage structure and their interaction with the Au NPs can be evinced by Raman spectroscopy. Such spectra show some characteristic peaks in the (600–1600) cm^{-1} region due to the presence of proteins, alanine, C–C, C–N, C–O, CH_2 and CH_3 chemical bonds. These peaks depend on the presence of the Au NPs, indicating that proteins and other molecules can be altered by their presence, as reported in the literature [12]. As an example, Figure 5a shows the X-ray image of the Au L fluorescence lines detected in the TEM image of Au NPs adherent to a phage filamentation (yellow dots), while Figure 5b shows a typical Raman spectrum in the (600–1800) cm^{-1} region of the phage with the Au NP solution.

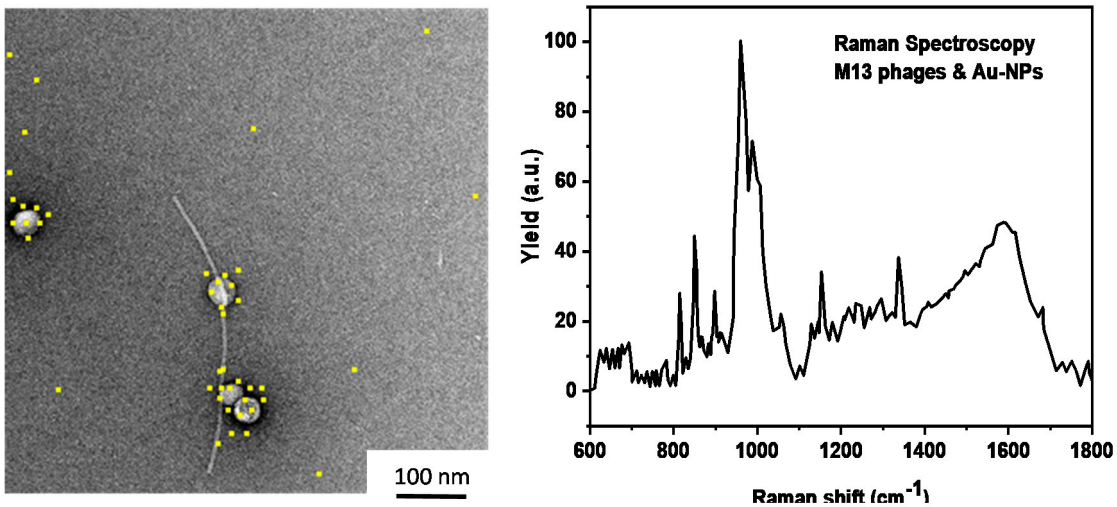

Figure 5. Characteristic X-ray image of the Au L lines in the TEM underlayer image (**a**) and typical Raman spectrum of the solution containing the M13 phages with Au NPs (**b**).

With respect to our previous measurements, some of which are published elsewhere [12], the advancements reported in this paper concern the use of solutions containing a different concentration of surfactant to reduce Au NPs coalescence, the different preparative of the SEM and TEM samples to better observe Au NPs adhesion to the M13 phages, the evaluation of the average number of nanoparticles adherent to the phages per unit of length and of the average size and shape of the produced NPs. Such investigation confirms the previous data analysis, i.e., that the Au NPs are bonded to the phages head and tail and to their lateral surface, and that the NPs are spherical and generally of an average size of about 20 nm. Such size and the spherical shape may confer high penetrability of the cell membrane; however, further investigation should be performed to assert that this size is the best.

The uptake effect seems high and limited to a maximum of about 12 particles/phage, a very low number with respect to that of nanoparticles immersed in the solution which is orders of magnitude higher. The performed measurements are only preliminary and up to now, do not allow to establish the level of stability of the Au NPs–phage adhesion. It probably depends on a combination of different factors, such as the time, the temperature, the PH of the biological liquids and by other effects which were not investigated in this paper.

5. Conclusions

In this work, the bonding effect of Au NPs to M13 phages was studied. Microscopy investigation has shown that each phage is capable to transport clusters of Au nanoparticles, generally attached to the filament terminations. The different number of Au NPs attached to the phages measured by SEM and TEM can be due to the different method of sample preparation for the two microscopies. The dimension of the Au NPs and of phages was measured by AFM and TEM images, which have also allowed to estimate the number of Au NPs bonded to the phages.

M13 phages, engineered to expose peptides able to specifically recognize tumor cells, can diffuse into the human body through the blood flux, moving from the extracellular to the intracellular membrane [30].

The phages, encountering Au NPs locally injected with a biological solution, can come in contact with them, and/or force some NPs to block where they are, or convey them through the flow into the cell and bring them close to the cell nucleus. In this way, it is possible employ the Au NPs transported by phages to localize them in tumoral cells. It is important take into account that the nanoparticles can be functionalized in order to adhere to the phages and with them, in fluids, reach the target (tumoral cells) in order to preserve the healthy cells. This can be possible by employing biocompatible and heavy elements, such as Au, which allow to increase the cell's effective atomic number and its electron density. The higher effective atomic number allows to deposit higher energy doses during radiotherapy both using traditional radiotherapy (X-rays and electrons) and innovative proton radiotherapy. In fact, both the absorption mass coefficient for X-rays and the ion and electron energy loss increase in targets with a high atomic number, depositing high energy and doses. Moreover, the use of the Au NPs at low concentration, below 1% in weight, allows to enhance the heat transport in cells during hyperthermia applications and to obtain a high contrast imaging of biological samples thanks to the fluorescence emission of the Au atoms and to the optical SPR effects [31]. Thus, if the hyperthermia process is obtained using lamps or lasers whose emitted radiation is transported to the tissue through light fibers, for example, it will be possible to enhance the temperature by the Au NPs absorbance band with a maximum value at the lamp or laser wavelength, obtaining good and local treatment of heat.

Author Contributions: L.T. and S.G. planned the experiments, performed, acquired and interpreted biological experiments. L.T. and A.T. collected the experimental data and revised the original manuscript. All authors (Physicists: L.T., L.S., V.L., M.C., L.K. and A.T., and Biologists: L.M.D.P., D.F. and S.G.) analyzed the results and prepared the manuscript. All authors have read and agreed to the published version of the manuscript.

Funding: This research received no external funding.

Institutional Review Board Statement: Not applicable.

Informed Consent Statement: Not applicable.

Acknowledgments: The authors wish to thank Franco Felici for the kind gift of phage display M13 libraries. Supported by OP RDE, MEYS, Czech Republic under the project CANAM OP, CZ.02.1.01/0.0/0.0/16_013/0001812.

Conflicts of Interest: The authors declare no conflict of interest.

References

1. Moghimian, P.; Srot, V.; Pichon, B.P.; Facey, S.J.; van Aken, P.A. Stability of M13 Phage in Organic Solvents. *J. Biomater. Nanobiotechnol.* **2016**, *7*, 72–77. [CrossRef]
2. Tsen, K.T.; Tsen, S.-W.D.; Fu, Q.; Lindsay, S.M.; Kibler, K.; Jacobs, B.; Wu, T.C.; Li, Z.; Yan, H.; Cope, S.; et al. Photonic Approach to the Selective Inactivation of Viruses with a Near-Infrared Ultrashort Pulsed Laser. In Proceedings of the SPIE Proceedings Optical BioS 2010, San Francisco, CA, USA, 23–28 January 2010; Robert, R., Ed.; SPIE: Washington, DC, USA, 2010; Volume 7561, p. 75610W.
3. Cui, Y. Engineered phages for electronics. *Biosens. Bioelectron.* **2016**, *85*, 964–976. [CrossRef] [PubMed]

4. Manivannan, S.; ParkJuwon, S.; Kim, J.K. Aggregation-free optical and colorimetric detection of Hg(II) with M13 bacteriophage-templated Au nanowires. *Biosens. Bioelectron.* **2020**, *161*, 112237. [CrossRef]
5. Derakhshanfar, S.; Mbeleck, R.; Xu, K.; Zhang, X.; Zhong, W.; Xing, M. 3D bioprinting for Biomedical devices and tissue engineering: A review of recent trends and advances. *Bioact. Mater.* **2018**, *3*, 144–156. [CrossRef]
6. Farr, R.; Choi, D.S.; Lee, S.-W. Phage-based nanomaterials for biomedical applications. *Acta Biomater.* **2014**, *10*, 1741–1750. [CrossRef] [PubMed]
7. Huh, H.; Wong, S.; Jean, J.S.; Slavcev, R. Bacteriophage interactions with mammalian tissue: Therapeutic applications. *Adv. Drug Deliv. Rev.* **2019**, *145*, 4–17. [CrossRef] [PubMed]
8. Barr, J.J. A bacteriophage journey through the human body. *Immunol. Rev.* **2017**, *279*, 106–122. [CrossRef] [PubMed]
9. Pasqualini, R.; Ruoslahti, E. Organ targeting in vivo using phage display peptide libraries. *Nature* **1996**, *380*, 364. [CrossRef]
10. Gillespie, J.W.; Yang, L.; De Plano, L.M.; Stackhouse, M.A.; Petrenko, V.A. Evolution of a landscape phage library in a mouse xenograft model of human breast cancer. *Viruses* **2019**, *11*, 988. [CrossRef] [PubMed]
11. Pokorski, J.K.; Steinmetz, N.F. The Art of Engineering Viral Nanoparticles. *Mol. Pharm.* **2011**, *8*, 29–43. [CrossRef] [PubMed]
12. Torrisi, L.; Guglielmino, S.; Silipigni, L.; De Plano, L.M.; Kovacik, L.; Lavrentiev, V.; Torrisi, A.; Fazio, M.; Fazio, B.; Di Marco, G. Study of gold nanoparticle transport by M13 phages towards Disease tissues as targeting procedure for radiotherapy applications. *Gold Bull.* **2019**, *52*, 135–144. [CrossRef]
13. Wang, X.Y.; Yang, J.Y.; Wang, Y.T.; Zhang, H.C.; Chen, M.L.; Yang, T.; Wang, J.H. M13 phage-based nanoprobe for SERS detection and inactivation of *Staphylococcus aureus*. *Talanta* **2021**, *221*, 121668. [CrossRef] [PubMed]
14. Dong, X.; Pan, P.; Zheng, D.W.; Bao, P.; Zeng, X.; Zhang, X.Z. Bioinorganic hybrid bacteriophage for modulation of intestinal microbiota to remodel tumor-immune microenvironment against colorectal cancer. *Sci. Adv.* **2020**, *6*, eaba1590. [CrossRef]
15. Kadhim, R.J.; Karsh, E.H.; Taqi, Z.J.; Jabir, M.S. Biocompatibility of gold nanoparticles: In-vitro and In-vivo study. *Mater. Today-Proc.* **2021**, *42*, 3041–3045. [CrossRef]
16. Hainfeld, J.F.; Lin, L.; Slatkin, D.N.; Dilmanian, F.A.; Vadas, T.M.; Smilowitz, H.M. Gold nanoparticle hyperthermia reduces radiotherapy dose. *Nanomedicine* **2014**, *10*, 1609–1617. [CrossRef] [PubMed]
17. Gaiduk, A.; Paul, V.; Ruijgrok, P.V.; Yorulmaz, M.; Orrit, M. Making gold nanoparticles fluorescent for simultaneous absorption and fluorescence detection on the single particle level. *Phys. Chem. Chem. Phys.* **2011**, *13*, 149–153. [CrossRef]
18. Torrisi, L.; Restuccia, N.; Cuzzocrea, S.; Paterniti, I.; Ielo, I.; Pergolizzi, S.; Cutroneo, M.; Kovacik, L. Laser-produced Au nanoparticles as X-ray contrast agents for diagnostic imaging. *Gold Bull.* **2017**, *50*, 51–60. [CrossRef]
19. Torrisi, L.; Restuccia, N.; Torrisi, A. Study of gold nanoparticles for mammography diagnostic and radiotherapy improvements. *Rep. Pract. Oncol. Radiother.* **2019**, *24*, 450–457. [CrossRef] [PubMed]
20. Torrisi, A.; Cutroneo, M.; Torrisi, L.; Vacík, J. Biocompatible nanoparticles production by pulsed laser ablation in liquids. *J. Instrum.* **2020**, *15*, C03053. [CrossRef]
21. Volkert, A.A.; Subramaniam, V.; Ivanov, M.R.; Goodman, A.M.; Haes, A.J. Salt-Mediated Self-Assembly of Thioctic Acid on Gold Nanoparticles. *ACS Nano* **2011**, *5*, 4570–4580. [CrossRef]
22. Wang, P.; Wang, X.; Wang, L.; Hou, X.; Liu, W.; Chen, C. Interaction of gold nanoparticles with proteins and cells. *Sci.Technol. Adv. Mater.* **2015**, *16*, 034610. [CrossRef]
23. Casals, E.; Pfaller, T.; Duschl, A.; Oostingh, G.J.; Puntes, V.F. Hardening of the nanoparticle-Protein corona in metal (Au, Ag) and oxide (Fe_3O_4, CoO, and CeO_2) nanoparticles. *Small* **2011**, *7*, 3479–3486. [CrossRef] [PubMed]
24. Deng, Z.J.; Liang, M.; Monteiro, M.; Toth, I.; Minchin, R.F. Nanoparticle-induced unfolding of fibrinogen promotes Mac-1 receptor activation and inflammation. *Nat. Nanotechnol.* **2011**, *6*, 39–44. [CrossRef] [PubMed]
25. Aubin-Tam, M.E.; Hamad-Schifferli, K. Gold nanoparticle-cytochrome C complexes: The effect of nanoparticle ligand charge on protein structure. *Langmuir* **2005**, *21*, 12080–12084. [CrossRef] [PubMed]
26. Torrisi, L. Evaluation of the Radiotherapy and Protontherapy improvement using gold nanoparticles. *Gold Bull.* **2017**, *50*, 299–311. [CrossRef]
27. Vines, J.B.; Yoon, J.H.; Ryu, N.E.; Lim, D.J.; Park, H. Gold Nanoparticles for Photothermal Cancer Therapy. *Front. Chem.* **2019**, *7*, 167. [CrossRef] [PubMed]
28. Torrisi, L.; Restuccia, N. Nanoparticles in Liquids generated by Laser as Contrast Medium and Radiotherapy Intensifiers. *EPJ Web Conf.* **2018**, *167*, 04007.
29. Torrisi, L.; Restuccia, N. Laser-Generated Au Nanoparticles for Bio-Medical Applications. *IRBM* **2018**, *39*, 307–312. [CrossRef]
30. Kim, A.; Shin, T.H.; Shin, S.M.; Pham, C.D.; Choi, D.K.; Kwon, M.H.; Kim, Y.S. Cellular internalization mechanism and intracellular trafficking of filamentous M13 phages displaying a cell-penetrating transbody and TAT peptide. *PLoS ONE* **2012**, *7*, e51813. [CrossRef]
31. Deb, P.K.; Odetallah, H.M.A.; Al-Jaidi, B.; Akkinepalli, R.R.; Al-Aboudi, A.; Tekade, R.K. Chapter 11—Biomaterials and Nanoparticles for Hyperthermia Therapy, Biomaterials and Bionanotechnology. *Adv. Pharm. Prod. Dev. Res.* **2019**, 375–413. [CrossRef]